Supporting Information

Interface Catalysts of Ni/Co_2N for Hydrogen Electrochemistry

Kaixi Sun[1,2#], Tong Zhang[2,3,4#], Liming Tan[2#], Dexia Zhou[5#], Yuqin Qian[2], Xiaoxia Gao[1], Fahui Song[1]*, Hongtao Bian[5]*, Zhou Lu[6]*, Jingshuang Dang[5], Hong Gao[3], Jeremy Shaw[1], Shutang Chen[7], Gugang Chen[7], and Yi Rao[2]*

[1]Key Laboratory of Pesticide & Chemical Biology Ministry of Education, College of Chemistry, Central China Normal University, Wuhan, Hubei 430079, China
[2]Department of Chemistry and Biochemistry, Utah State University, USA
[3]Beijing National Laboratory for Molecular Sciences and State Key Laboratory of Molecular Reaction Dynamics, Institute of Chemistry, Chinese Academy of Sciences, Beijing 100190, China
[4]University of Chinese Academy of Sciences, Beijing 100049, China
[5]Key Laboratory of Applied Surface and Colloid Chemistry, Ministry of Education, School of Chemistry and Chemical Engineering, Shaanxi Normal University, Xi'an, 710119, China
[6]Anhui Province Key Laboratory of Optoelectronic Material Science and Technology School of Physics of Electronic Information, Anhui Normal University, Wuhu, Anhui, China 241002
[7]Honda Research Institute, USA, Inc., San Jose, CA 95134, USA

Corresponding authors: yi.rao@usu.edu (Y.R.); fhsong@mail.ccnu.edu.cn (F.H.S.); htbian@snnu.edu.cn (H.T.B.); zhoulu@ahnu.edu.cn (Z.L.).

[#] K.S., T.Z., L.T., and D.Z. contributed equally to this work.

1. Experimental section

Materials. Ammonium chloride was purchased from Damao Chemical Reagent Factory. Nickle chloride was purchased from Sinopharm Chemical Reagent Co., Ltd. Cobalt chloride was purchased from Tianjin Standard Technology Co., Ltd. Ammonium carbonate was purchased from Sinopharm Chemical Reagent Co., Ltd. Nickel foam was purchased from MTI. Potassium hydroxide was purchased from Sinopharm Chemical Reagent Co., Ltd. Commercial Pt/C catalyst (20% Pt on Vulcan XC-72) was purchased from Premetek. All chemicals were used as received without any further purification. Water deionized was used in all experiments.

Synthesis. The Ni/Co_2N catalysts were prepared by a facile template-free cathodic electrodeposition of porous Ni and Co microsphere arrays on nickel foam, followed by low-temperature ammonium carbonate treatment. Typically, the electrodeposition of 3D porous Ni and Co microspheres on nickel foam (NiCo) was performed in a standard two-electrode glass cell at room temperature with an electrolyte consisting of 2.0 M NH_4Cl and 0.1 M $NiCl_2$ and $CoCl_2$. A piece of commercial nickel foam with a size of 0.5 cm by 0.5 cm was used as the working electrode and a Pt wire as the counter electrode. The electrodeposition was carried out at a constant current density of -1.0 A cm^{-2} for 500 s to obtain NiCo samples. Subsequently, the resulting NiCo was placed at the center of a tube furnace, and 4.2 g of $(NH_4)_2CO_3$ was placed at the upstream side and near to NiCo. After it was flushed with Ar gas, the center of the furnace was quickly elevated to the reaction temperature of 420 ℃ with a ramping rate of 10 ℃ min^{-1} and kept at 420 ℃ for 0.5 h. After the system was cooled to room temperature, the final product denoted as Ni/Co_2N was obtained.

Characterization. Scanning electron microscopy (SEM) measurements were collected on a Hitachi SU8220. X-ray diffraction (XRD) patterns were obtained on a Rigaku MinifexII Desktop X-ray diffractometer. The X-ray photoelectron spectroscopy analyses were performed using a Kratos Axis Ultra instrument (Kratos Analytical Ltd.) at the Shaanxi Normal University. High Resolution Transmission Electron Microscopy (HR-TEM) measurements were collected on a JEM-2100.

Electrochemical Measurements. Electrochemical measurements were performed by a computer controlled PGSTAT302N electrochemical workstation with a three-electrode cell system and a scan rate of 5 mV s^{-1}. The resulting NiCo, Pt/NF, Ni/Co_2N or NF were used as the working electrode, a SCE electrode as the reference electrode, and a Pt wire as the counter electrode. The electrolyte for HER and OER was 1.0 M KOH. The electrolyte for HOR was 0.1 M KOH. All potentials reported herein are quoted with respect to the reversible hydrogen electrode (RHE) through RHE calibration.

For overall water splitting tests, the Ni/Co_2N was used as both an anode and a cathode electrode. The potential scan range was from 0 to 2.1 V. iR (current times internal resistance) compensation was applied in all the electrochemical experiments to account for the voltage drop between the reference and working electrodes using Nova 2.1 Data Acquisition Software. Electrochemical double layer capacitance (Cdl) of the resulting electrocatalysts was evaluated by using cyclic voltammetry in a non-Faradaic region at different scan rates of 10, 20, 30, 40, and 50 mV s^{-1}. From a plot of the difference between the anodic and cathodic current densities at the middle potential versus scan rate, the resulting linear slope is twice the Cdl value.

For HOR tests, the steady-state measurements were conducted to obtain the polarization curves instead of LSV or CV methods to minimize the capacitive current background. The multi-step CA was conducted at a potential window from −0.05 to 0.1 V vs. RHE with a 5 mV interval for every 60 s. The stable anodic current recorded at 60 s under each potential was used to plot the steady-state polarization curves for HOR.

2. Computational Details

Density functional theory (DFT) calculations were performed using the Vienna Ab Initio Simulation Package (VASP). Exchange-correlation energies were determined by using the Perdew–Burke–Ernzerhof (PBE) model of generalized gradient approximation (GGA). The Projector Augmented-Wave (PAW) method with a plane wave cut-off energy of 450 eV was used for total energy calculations. The convergence thresholds for energy and force were set as 10^{-4} eV and 0.04 eV/Å, respectively, and the Brillouin zones were sampled by the Monkhorst−Pack k-point meshes. The surface of Ni (1-10) and Co_2N(100) was modeled using a 2 × 1 surface slab cell with a vacuum of 10 Å. For interface models, a 10 Å vacuum slab was used. Once the slab models were optimized all subsequent calculations were performed with the bottom four layers fixed.

A typical descriptor of the rate of the overall reaction is the adsorption free energy of H and expressed as follows:

$$\Delta G_{H*}=\Delta E_H+\Delta E_{ZPE}-T\Delta S_H$$

Where ΔE_{ZPE} is the difference in zero point energy between the adsorbed and the gaseous H, ΔS_H is the corresponding change of entropy, and ΔE_H is the hydrogen chemi-sorptions energy which is computed as follows: ΔE_H = E(surface +H)-E(surface)+1/2 E(H_2). Where E(surface +H), E(surface), E(H_2) are energies of the surface with adsorbed hydrogen atom, clean surface and molecular hydrogen, respectively. ΔE_{ZPE} can be obtained by frequency analysis followed by geometry optimization. ΔS_H can be estimated by -1/2ΔS_{H2} assuming the vibration entropy of the adsorbate is small, where ΔS_{H2} is the entropy of H_2.

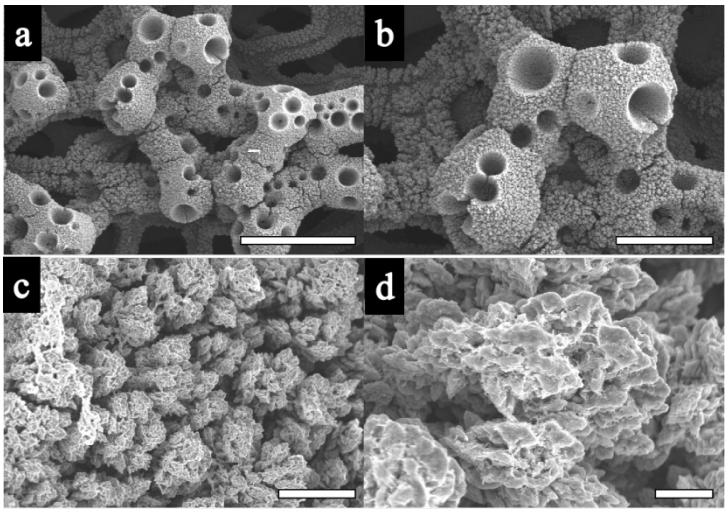

Figure S1. a-d SEM images of NiCo under different magnifications (**a**:500μm; **b**:300μm; **c**:10μm; **d**:2μm).

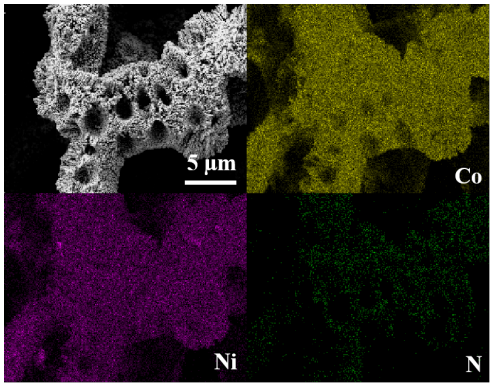

Figure S2. SEM images for a total of Co, Ni, and N elemental mapping, Co, Ni, and N elemental mappings in Ni/Co_2N.

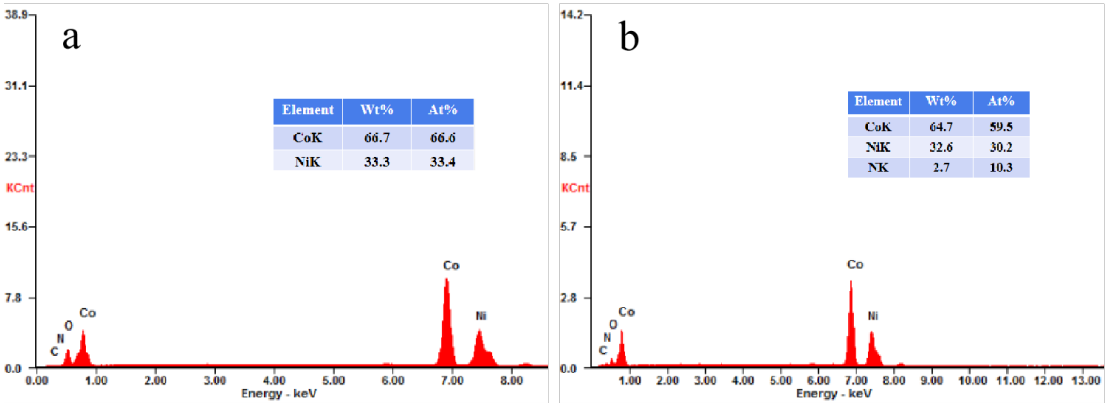

Figure S3. EDX spectra of NiCo (**a**) and Ni/Co_2N (**b**).

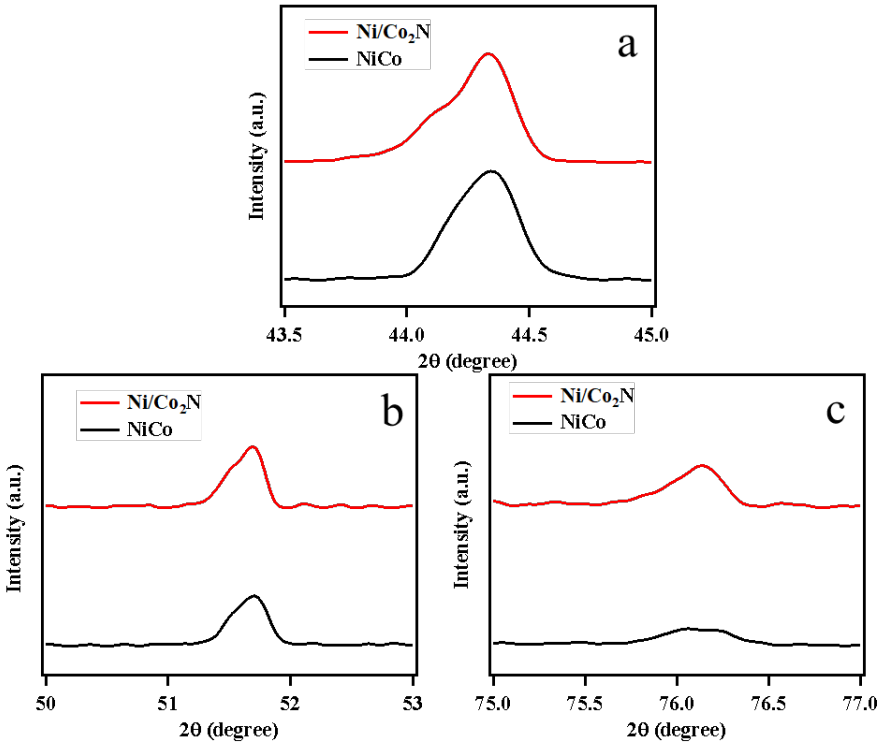

Figure S4. XRD patterns of Ni/Co_2N and NiCo within fine angles.

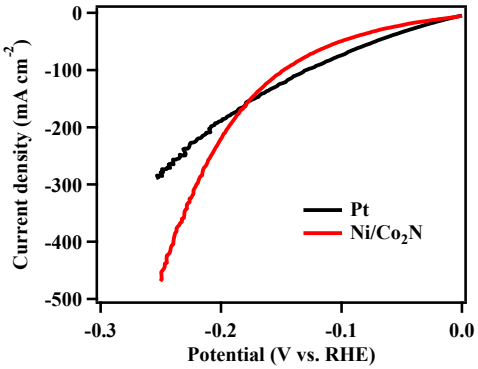

Figure S5. iR-corrected polarization curves of Ni/Co_2N and Pt/NF (Pt/C: 0.5 mg cm^{-2}) in 1.0 M KOH.

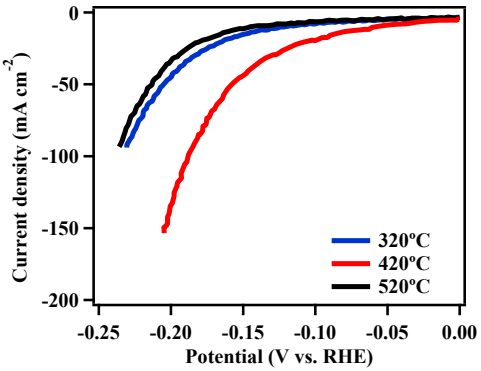

Figure S6. iR-corrected polarization curves of Ni/Co_2N synthesized at different temperatures for 0.5 h. The polarization curves were collected in 1.0 M KOH.

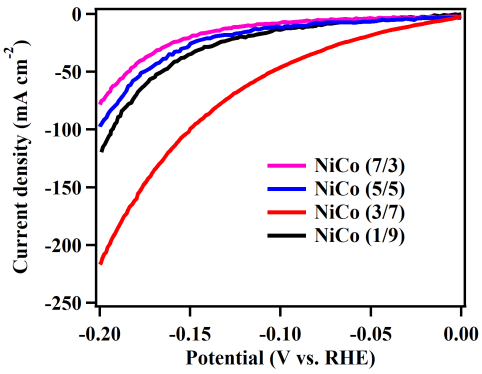

Figure S7. iR-corrected polarization curves of Ni/Co_2N with different Ni/Co molar ratios synthesized at 350°C for 0.5 h. The polarization curves were collected in 1.0 M KOH.

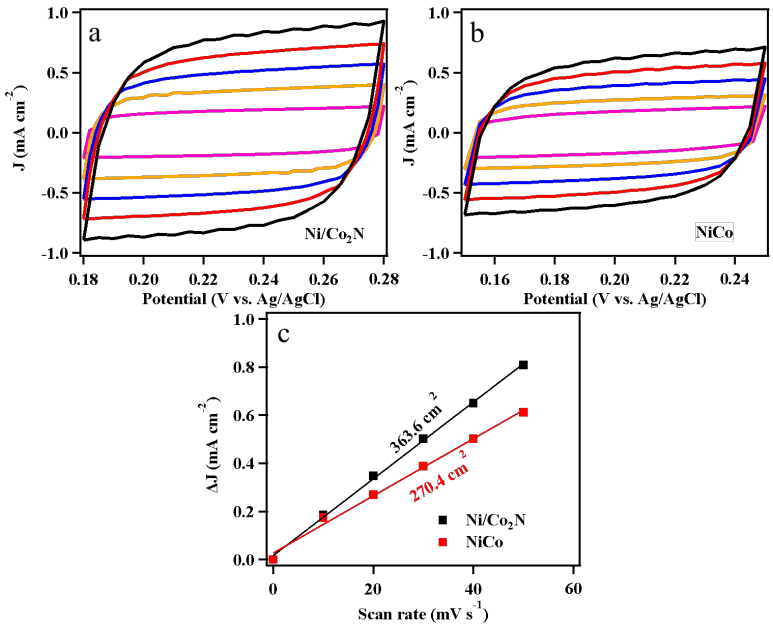

Figure S8. Electrochemically active surface area (ECSA) measurements. CV curves of Ni/Co_2N (a) and NiCo (b) collected at various scan rates ranging from 10 to 50 mV s^{-1} in CH_3CN with 0.15 M KPF_6. c) The linear fitting of scan rate versus ΔJ (the difference between the anodic and cathodic current densities at open circuit potential).

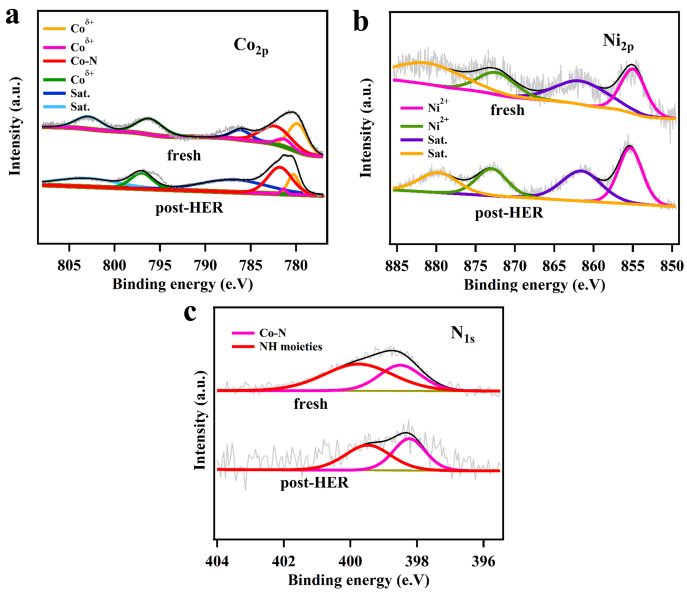

Figure S9. XPS spectra of Co 2p, Ni 2p, and N 1s for Ni/Co_2N before and after HER electrocatalysis.

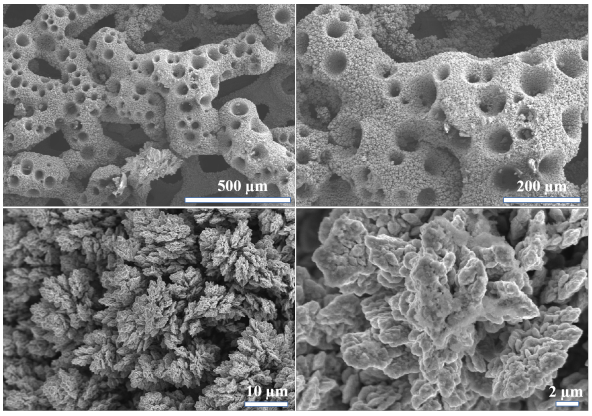

Figure S10. SEM images of for Ni/Co_2N after HER electrocatalysis.

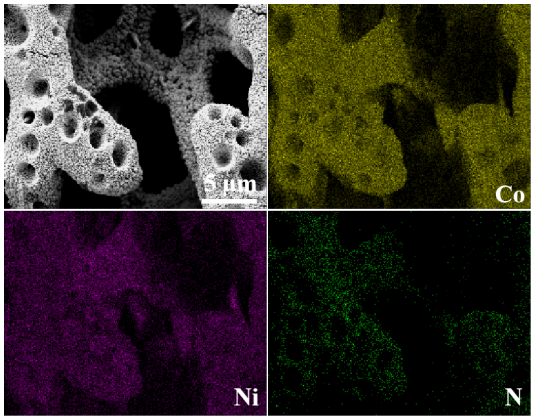

Figure S11. Elemental mapping images of for Ni/Co_2N after HER electrocatalysis.

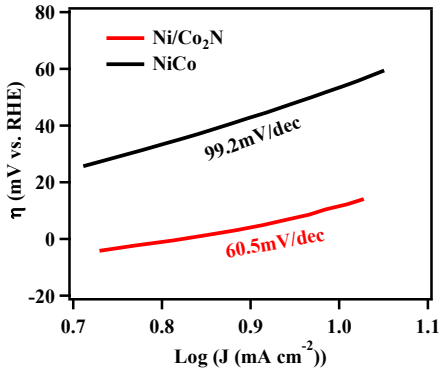

Figure S12. Tafel plots of Ni/Co_2N and NiCo in 1.0 M KOH.

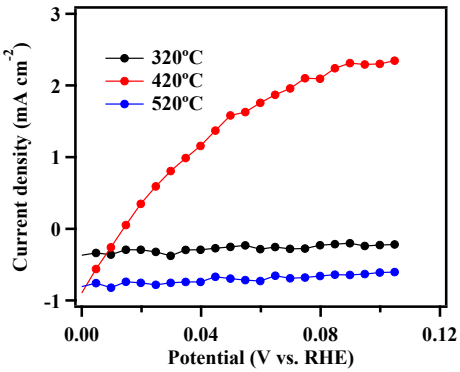

Figure S13. Steady-state polarization curves of Ni/Co_2N at different temperatures in H_2-saturated 0.1 M KOH (pH=13).

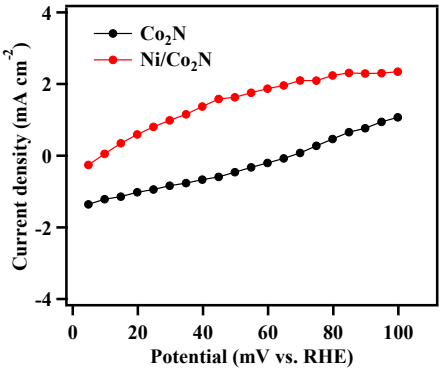

Figure S14. Steady-state polarization curves of Ni/Co_2N and Co_2N in H_2-saturated 0.1 M KOH (pH=13).

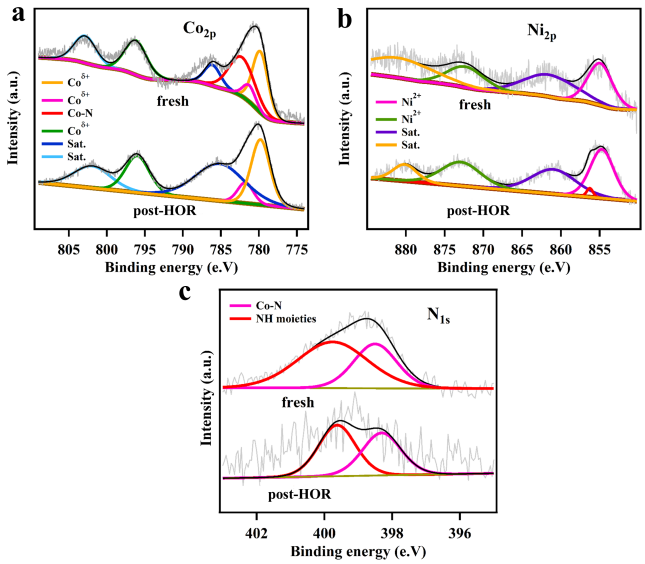

Figure S15. XPS spectra of Co 2p, Ni 2p, and N 1s for Ni/Co_2N before and after HOR electrocatalysis.

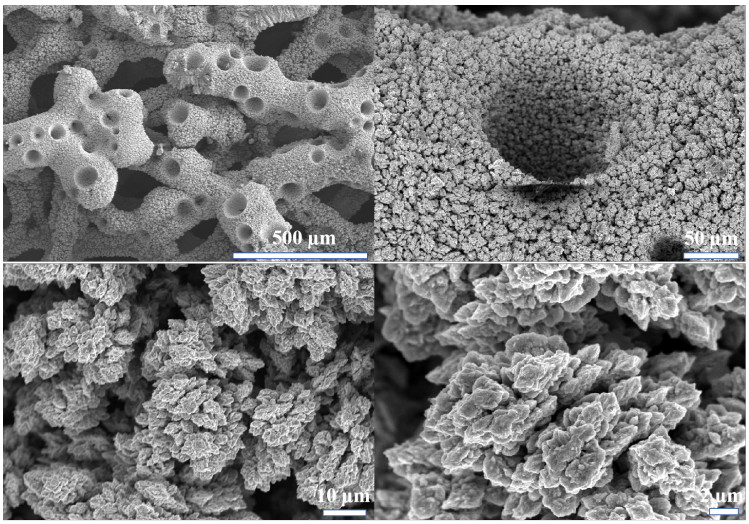

Figure S16. SEM images of for Ni/Co_2N after HOR electrocatalysis.

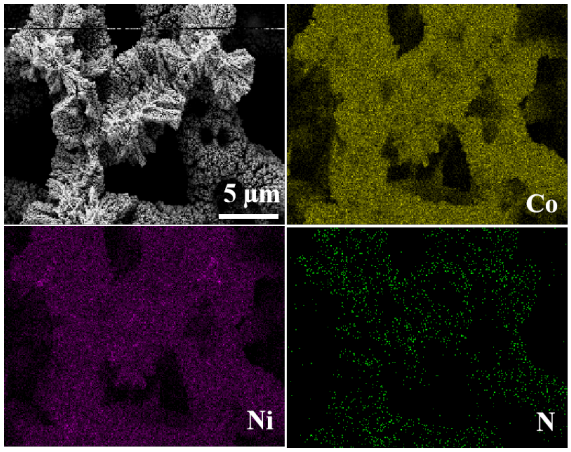

Figure S17. Elemental mapping images of for Ni/Co_2N after HOR electrocatalysis.

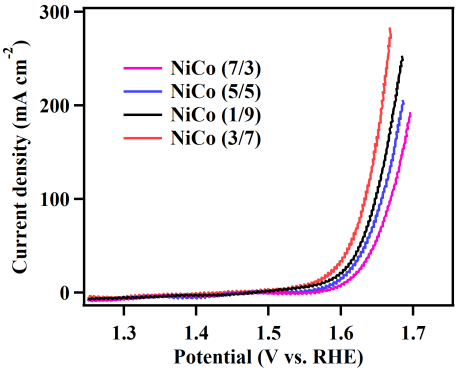

Figure S18. iR-corrected polarization curves of Ni/Co_2N with different Ni/Co molar ratios synthesized at 350°C for 0.5 h. The polarization curves were collected in 1.0 M KOH.

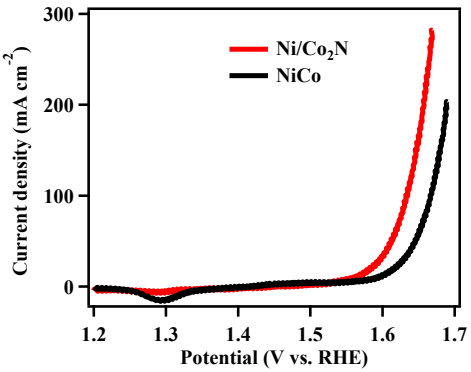

Figure S19. iR-corrected polarization curves of Ni/Co_2N and NiCo in 1.0 M KOH (pH=14).

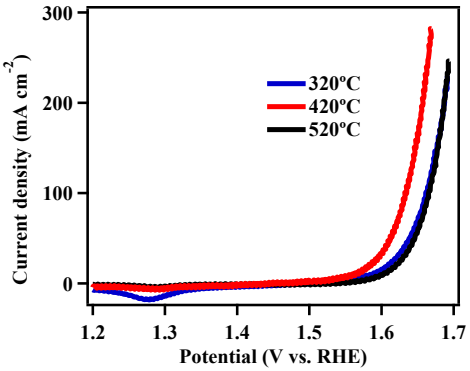

Figure S20. iR-corrected polarization curves of Ni/Co_2N synthesized at different temperatures for 0.5 h. The polarization curves were collected in 1.0 M KOH (pH=14).

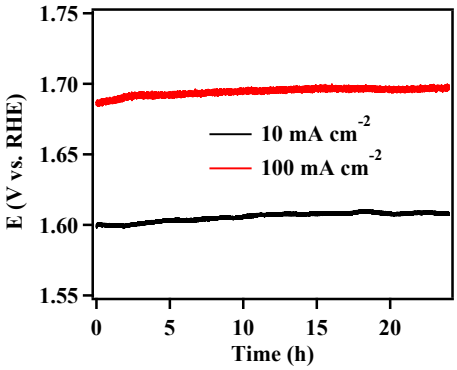

Figure S21. Chronopotentiometric curves of Ni/Co_2N at 10 and 100 mA cm^{-2} in 1.0 M KOH (pH=14).

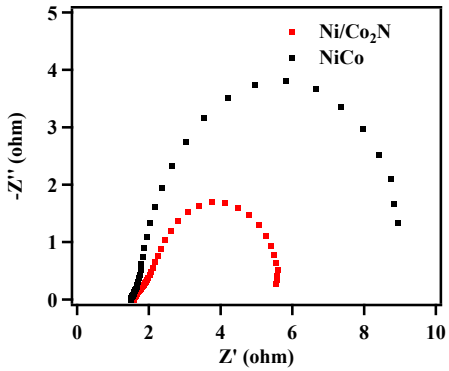

Figure S22. Nyquist plots of Ni/Co_2N and NiCo measured at 1.567 V vs. RHE in 1.0 M KOH.

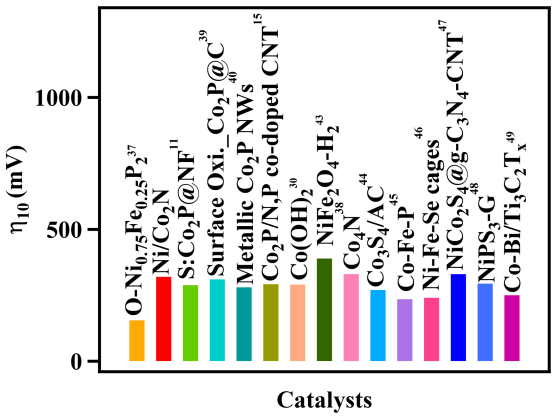

Figure S23. Comparison of the OER performance for Ni/Co_2N with those reported in the literature.

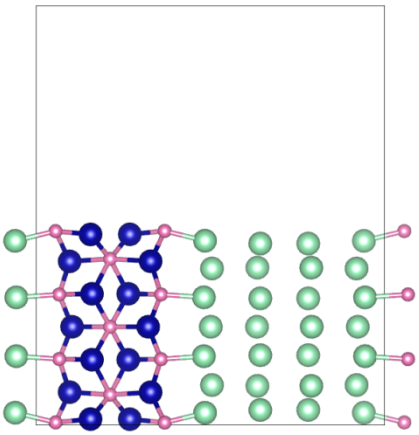

Figure S24. Structure of Ni/Co_2N interface (side view).

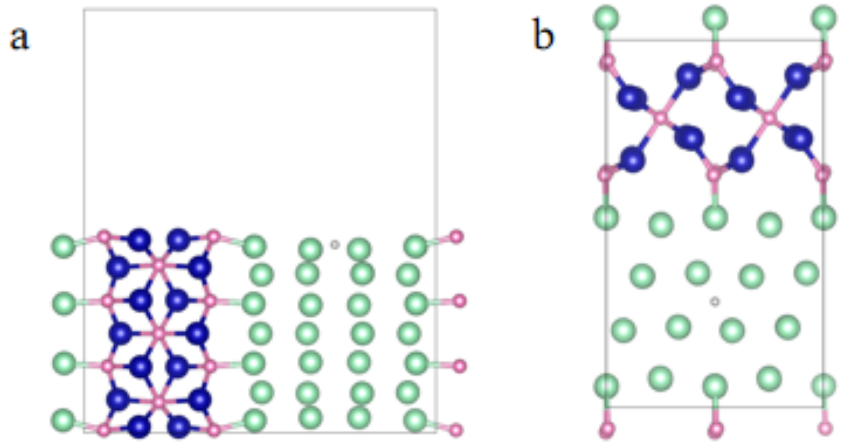

Figure S25. Adsorption structures of hydrogen onto Ni/Co_2N_Ni. (a) side view and (b) top view.

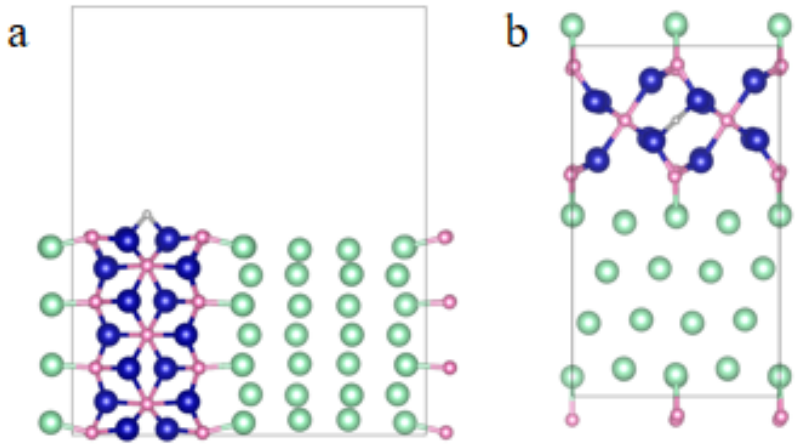

Figure S26. Adsorption structures of hydrogen onto Ni/Co_2N_Co. (a) side view and (b) top view.

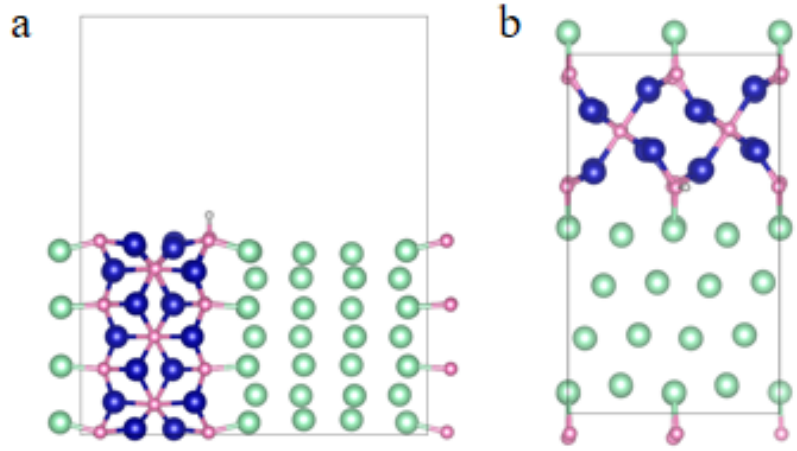

Figure S27. Adsorption structures of hydrogen onto Ni/Co_2N_N. (a) side view and (b) Top view.

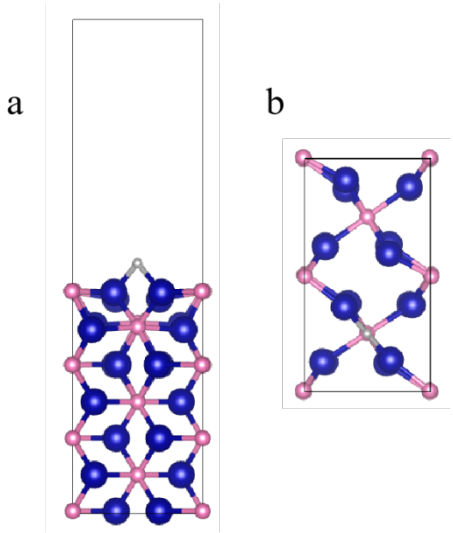

Figure S28. Adsorption structures of hydrogen onto Co_2N. (a) side view and (b) top view.

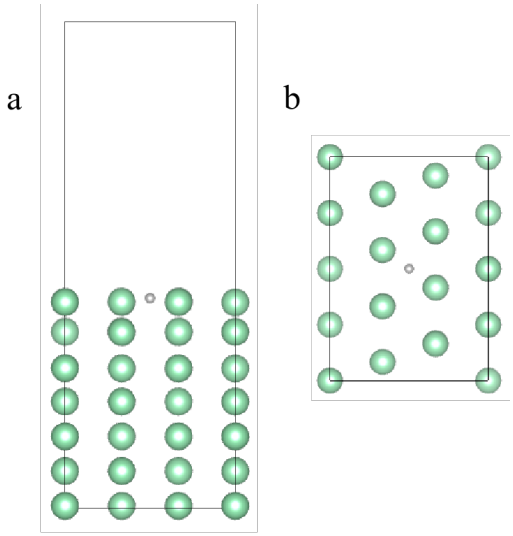

Figure S29. Adsorption structures of hydrogen onto Ni. (a) side view and (b) top view.

Table S1 Comparison of electrocatalytic HER activity of various nonprecious catalysts in 1.0 M KOH electrolyte with those reported in the literature.

Catalysts	**J (mA cm^{-2})**	**η (mV)**	**Reference**
Ni/Co_2N	10	-16.2	This work
Ni_2P/Ni/NF	10 20	-98 -120	Ref 1
MoC_x/C	10	-151	Ref 2
CoO_x@CN	10	-232	Ref 3
MoS_{2+x}/FTO	10	-310	Ref 4
CoP/CC	10	-209	Ref 5
Co-NRCNTs	10	-370	Ref 6
Ni_2P	20	-205	Ref 7
FeP NAs/CC	10	-218	Ref 8
NiS_2/MoS_2 HNW	10	-204	Ref 9
NiMoN	10	-109	Ref 10
S:Co_2P@NF	10	-105	Ref 11
S-MoP NPL	10	-104	Ref 12
N-$NiCo_2S_4$	10	-41	Ref 13
Ni_4Mo	10	-35	Ref 14
$CoP_{2x}Se_{2(1-x)}$	10	-98	Ref 30
Ni–W–O/$NiMoO_4$-1	10	-52	Ref 31
SLG/FLG-DE	10	-85	Ref 32
NiO/Al_3Ni_2	10	-66	Ref 33
N−Ni	10	-95	Ref 34
PANI/Ni/NF	10	-72	Ref 35
NiMo-NWs/Ni-foam	10	-30	Ref 36

Table S2 Comparison of electrocatalytic OER activity of various nonprecious catalysts with those reported in the literature.

Catalysts	J (mA cm^{-2})	η (mV)	Electrolyte	Reference
Ni/Co_2N	10	320	1.0M KOH	This work
O-$Ni_{0.75}Fe_{0.25}P_2$	10	155	1.0M KOH	Ref 37
Co_4N	10	330	1.0M KOH	Ref 38
S:Co_2P@NF	10	288	1.0M KOH	Ref 11
Surface Oxi.-Co_2P@C	10	310	1.0M KOH	Ref 39
Metallic Co_2P NWs	10	280	1.0M KOH	Ref 40
Co_2P/N,P co-doped CNT	10	292	1.0M KOH	Ref 15
$Co(OH)_2$	10	290	1.0M KOH	Ref 30
CoO/CoxP	10	370	0.1M KOH	Ref 41
(Co,Fe)3N_2D	10	310	0.1M KOH	Ref 42
$NiFe_2O_4$−H_2	10	389	1.0M KOH	Ref 43
Co3S4/AC	10	270	1.0M KOH	Ref 44
Co-Fe-P	10	235	1.0M KOH	Ref 45
Ni–Fe–Se cages	10	240	1.0M KOH	Ref 46
$NiCo_2S_4$@g‐C_3N_4‐CNT	10	330	1.0M KOH	Ref 47
$NiPS_3$-G	10	294	1.0M KOH	Ref 48
Co-Bi/$Ti_3C_2T_x$	10	250	1.0M KOH	Ref 49

Table S3. Comparison with overpotential η_{10} in various electrocatalysts for overall water splitting with those reported in the literature.

Material	**η_{10} (mV)**	**η_{100} (mV)**	**Reference**
Ni/Co_2N	340	530	This work
S-Co_2P-S-Co_2P@NF	400	567	Ref 11
Co_2P/N, P co-doped CNT	424		Ref 15
CoP/TM	410		Ref 16
Co-P film	420		Ref 17
Co_1Mn_1CH/NF	450		Ref 18
NiFe-OH-PO_4/NF	450		Ref 19
Amorphous CoSe film/Ti	420		Ref 20
CoP-MNA/Ni Foam	390		Ref 21
$NiCo_2Se_4$ holey nanosheets	450		Ref 22
Ni_2P nanoparticle	400		Ref 23
$NixFe_{3-x}$-O/NF	410		Ref 24
Hollow Co_3O_4 MTA	400		Ref 25
Co_3O_4 NC/CFP	680		Ref 26
$NiCo_2S_4$ NA/CC	450		Ref 27
CoS_x/Ni_3S_2@NF	342		Ref 28
NiCoP/CC	290	540	Ref 29
Ni_2P/Ni/NF	260	450	Ref 1

References

1. You, B.; Jiang, N.; Sheng, M.; Bhushan, M. W.; Sun, Y., Hierarchically Porous Urchin-Like Ni2P Superstructures Supported on Nickel Foam as Efficient Bifunctional Electrocatalysts for Overall Water Splitting. *ACS Catal.* **2016,** *6* (2), 714-721.
2. Wu, H. B.; Xia, B. Y.; Yu, L.; Yu, X.-Y.; Lou, X. W., Porous Molybdenum Carbide Nano-Octahedrons Synthesized via Confined Carburization in Metal-Organic Frameworks for Efficient Hydrogen Production. *Nat. Commun.* **2015,** *6* (1), 6512.
3. Jin, H.; Wang, J.; Su, D.; Wei, Z.; Pang, Z.; Wang, Y., In situ Cobal−Cobalt Oxide/N-Doped Carbon Hybrids As Superior Bifunctional Electrocatalysts for Hydrogen and Oxygen Evolution. *J. Am. Chem. Soc*. **2015,** *137*, 2688-2694.
4. Morales-Guio, C. G.; Liardet, L.; Mayer, M. T.; Tilley, S. D.; Grätzel, M.; Hu, X., Photoelectrochemical Hydrogen Production in Alkaline Solutions Using Cu2O Coated with Earth-Abundant Hydrogen Evolution Catalysts. *Angew. Chem. Int. Ed.* **2015,** *54*, 664-667.
5. Tian, J.; Liu, Q.; Asiri, A. M.; Sun, X., Self-Supported Nanoporous Cobalt Phosphide Nanowire Arrays: An Efficient 3D Hydrogen-Evolving Cathode over the Wide Range of pH 0–14. *J. Am. Chem. Soc*. **2014,** *136*, 7587-7590.
6. Zou, X.; Huang, X.; Goswami, A.; Silva, R.; Sathe, B. R.; Mikmeková, E.; Asefa, T., Cobalt-Embedded Nitrogen-Rich Carbon Nanotubes Efficiently Catalyze Hydrogen Evolution Reaction at All pH Values. *Angew.Chem. Int. Ed*. **2014,** *53*, 4372-4376.
7. Popczun, E. J.; McKone, J. R.; Read, C. G.; Biacchi, A. J.; Wiltrout, A. M.; Lewis, N. S.; Schaak, R. E., Nanostructured Nickel Phosphide as an Electrocatalyst for the Hydrogen Evolution Reaction. *J. Am. Chem. Soc*. **2013,** *135*, 9267-9270.
8. Liang, Y.; Liu, Q.; Asiri, A. M.; Sun, X.; Luo, Y., Self-Supported FeP Nanorod Arrays: A Cost-Effective 3D Hydrogen Evolution Cathode with High Catalytic Activity. *ACS Catal.* **2014,** *4*, 4065-4069.
9. Kuang, P.; Tong, T.; Fan, K.; Yu, J., In Situ Fabrication of Ni–Mo Bimetal Sulfide Hybrid as an Efficient Electrocatalyst for Hydrogen Evolution over a Wide pH Range. *ACS Catal*. **2017,** *7*, 6179−6187.
10. Zhang, Y.; Ouyang, B.; Xu, J.; Chen, S.; Rawat, R. S.; Fan, H. J., 3D Porous Hierarchical Nickel–Molybdenum Nitrides Synthesized by RF Plasma as Highly Active and Stable Hydrogen-Evolution-Reaction Electrocatalysts. *Adv. Energy Mater.* **2016,** *6*, 1600221.
11. Anjum, M. A. R.; Bhatt, M. D.; Lee, M. H.; Lee, J. S., Sulfur-Doped Dicobalt Phosphide Outperforming Precious Metals as a Bifunctional Electrocatalyst for Alkaline Water Electrolysis. *Chem. Mater.* **2018,** *30*, 8861−8870.
12. Liang, K.; Pakhira, S.; Yang, Z.; Nijamudheen, A.; Ju, L.; Wang, M.; Aguirre-Velez, C. I.; Sterbinsky, G. E.; Du, Y.; Feng, Z.; Mendoza-Cortes, J. L.; Yang, Y., S-Doped MoP Nanoporous Layer Toward High-Efficiency Hydrogen Evolution in pH-Universal Electrolyte. *ACS Catal.* **2019,** *9*, 651−659.
13. Wu, Y.; Liu, X.; Han, D.; Song, X.; Shi, L.; Song, Y.; Niu, S.; Xie, Y.; Cai, J.; Wu, S.; Kang, J.; Zhou, J.; Chen, Z.; Zheng, X.; Xiao, X.; Wang, G., Electron Density Modulation of NiCo2S4 Nanowires by Nitrogen Incorporation for Highly Efficient Hydrogen Evolution Catalysis. *Nat. Commun.* **2018,** *9*, 1425.
14. Zhang, Q.; Li, P.; Zhou, D.; Chang, Z.; Kuang, Y.; Sun, X., Superaerophobic Ultrathin Ni–Mo

Alloy Nanosheet Array from In Situ Topotactic Reduction for Hydrogen Evolution Reaction. *Small*, **2017,** *13*, 1701648.
15. Das, D.; Nanda, K. K., One-step, Integrated Fabrication of Co2P Nanoparticles Encapsulated N, P Dual-doped CNTs for Highly Advanced Total Water Splitting. *Nano Energy* **2016,** *30*, 303-311.
16. Yang, L.; Qi, H.; Zhang, C.; Sun, X., An Efficient Bifunctional Electrocatalyst for Water Splitting Based on Cobalt Phosphide. *Nanotechnol.* **2016,** *27* (23), 23LT01.
17. Jiang, N.; You, B.; Sheng, M.; Sun, Y., Electrodeposited Cobalt-Phosphorous-Derived Films as Competent Bifunctional Catalysts for Overall Water Splitting. *Angew. Chem., Int. Ed.* **2015,** *54* (21), 6251-6254.
18. Tang, T.; Jiang, W.-J.; Niu, S.; Liu, N.; Luo, H.; Chen, Y.-Y.; Jin, S.-F.; Gao, F.; Wan, L.-J.; Hu, J.-S., Electronic and Morphological Dual Modulation of Cobalt Carbonate Hydroxides by Mn Doping toward Highly Efficient and Stable Bifunctional Electrocatalysts for Overall Water Splitting. *J. Am. Chem. Soc.* **2017,** *139* (24), 8320-8328.
19. Lei, Z.; Bai, J.; Li, Y.; Wang, Z.; Zhao, C., Fabrication of Nanoporous Nickel–Iron Hydroxylphosphate Composite as Bifunctional and Reversible Catalyst for Highly Efficient Intermittent Water Splitting. *ACS Appl. Mater. Interfaces* **2017,** *9* (41), 35837-35846.
20. Liu, T.; Liu, Q.; Asiri, A. M.; Luo, Y.; Sun, X., An Amorphous CoSe Film Behaves as an Active and Stable Full Water-splitting Electrocatalyst Under Strongly Alkaline Conditions. *Chem. Commun.* **2015,** *51* (93), 16683-16686.
21. Zhu, Y.-P.; Liu, Y.-P.; Ren, T.-Z.; Yuan, Z.-Y., Self-Supported Cobalt Phosphide Mesoporous Nanorod Arrays: A Flexible and Bifunctional Electrode for Highly Active Electrocatalytic Water Reduction and Oxidation. *Adv. Funct. Mater.* **2015,** *25* (47), 7337-7347.
22. Fang, Z.; Peng, L.; Lv, H.; Zhu, Y.; Yan, C.; Wang, S.; Kalyani, P.; Wu, X.; Yu, G., Metallic Transition Metal Selenide Holey Nanosheets for Efficient Oxygen Evolution Electrocatalysis. *ACS Nano* **2017,** *11* (9), 9550-9557.
23. Stern, L.-A.; Feng, L.; Song, F.; Hu, X., Ni2P as a Janus Catalyst for Water Splitting: the Oxygen Evolution Activity of Ni2P Nanoparticles. *Energy Environ. Sci.* **2015,** *8* (8), 2347-2351.
24. Dong, C.; Kou, T.; Gao, H.; Peng, Z.; Zhang, Z., Eutectic-Derived Mesoporous Ni-Fe-O Nanowire Network Catalyzing Oxygen Evolution and Overall Water Splitting. *Adv. Energy Mater.* **2018,** *8* (5) 1701347.
25. Zhu, Y. P.; Ma, T. Y.; Jaroniec, M.; Qiao, S. Z., Self-Templating Synthesis of Hollow Co3O4 Microtube Arrays for Highly Efficient Water Electrolysis. *Angew. Chem. Int. Ed.* **2017,** *56* (5), 1324-1328.
26. Du, S.; Ren, Z.; Zhang, J.; Wu, J.; Xi, W.; Zhu, J.; Fu, H., Co3O4 Nanocrystal Ink Printed on Carbon Fiber Paper as a Large-area Electrode for Electrochemical Water Splitting. *Chem. Commun*, **2015,** *51*, 8066-8069.
27. Liu, D.; Lu, Q.; Luo, Y.; Sun, X.; Asiri, A. M., NiCo2S4 Nanowires Array as an Efficient Bifunctional Electrocatalyst for Full Water Splitting with Superior Activity. *Nanoscale,* **2015,** *7*, 15122-15126.
28. Shit, S.; Chhetri, S.; Jang, W.; Murmu, N. C.; Koo, H.; Samanta, P.; Kuila, T., Cobalt Sulfide/Nickel Sulfide Heterostructure Directly Grown on Nickel Foam: An Efficient and Durable Electrocatalyst for Overall Water Splitting Application. *ACS Appl. Mater. Interfaces* **2018,** *10*, 27712−27722.
29. Du, C.; Yang, L.; Yang, F.; Cheng, G.; Luo, W., Nest-like NiCoP for Highly Efficient Overall

Water Splitting. *ACS Catal.* **2017,** *7*, 4131−4137.
30. Liu, K.; Wang, F.; Shifa, T. A.; Wang, Z.; Xu, K.; Zhang, Y.; Cheng, Z.; Zhan, X.; He, J., An Efficient Ternary CoP2xSe2(1−x) Nanowire Array for Overall Water Splitting. *Nanoscale* **2017,** *9* (11), 3995-4001.
31. Liu, Y.; Wang, F.; Shifa, T. A.; Li, J.; Tai, J.; Zhang, Y.; Chu, J.; Zhan, X.; Shan, C.-X.; He, J., Hierarchically Heterostructured Metal Hydr(oxy)oxides for Efficient Overall Water Splitting. *Nanoscale* **2019,** *11*.
32. Najafi, L.; Bellani, S.; Oropesa-Nuñez, R.; Martín-García, B.; Prato, M.; Bonaccorso, F., Single-/Few-Layer Graphene as Long-Lasting Electrocatalyst for Hydrogen Evolution Reaction. *ACS Appl. Energy Mater.* **2019,** *2* (8), 5373-5379.
33. Zhou, Y.; Liu, H.; Zhu, S.; Liang, Y.; Wu, S.; Li, Z.; Cui, Z.; Chang, C.; Yang, X.; Inoue, A., Highly Efficient and Self-Standing Nanoporous NiO/Al3Ni2 Electrocatalyst for Hydrogen Evolution Reaction. *ACS Appl. Energy Mater.* **2019,** *2* (11), 7913-7922.
34. Jin, H.; Liu, X.; Chen, S.; Vasileff, A.; Li, L.; Jiao, Y.; Song, L.; Zheng, Y.; Qiao, S.-Z., Heteroatom-Doped Transition Metal Electrocatalysts for Hydrogen Evolution Reaction. *ACS Energy Lett.* **2019,** *4* (4), 805-810.
35. Song, F.; Li, W.; Han, G.; Sun, Y., Electropolymerization of Aniline on Nickel-Based Electrocatalysts Substantially Enhances Their Performance for Hydrogen Evolution. *ACS Appl. Energy Mater.* **2018,** *1* (1), 3-8.
36. Fang, M.; Gao, W.; Dong, G.; Xia, Z.; Yip, S.; Qin, Y.; Qu, Y.; Ho, J. C., Hierarchical NiMo-based 3D Electrocatalysts for Highly-efficient Hydrogen Evolution in Alkaline Conditions. *Nano Energy* **2016,** *27*, 247-254.
37. Liu, K.; Wang, F.; He, P.; Shifa, T. A.; Wang, Z.; Cheng, Z.; Zhan, X.; He, J., The Role of Active Oxide Species for Electrochemical Water Oxidation on the Surface of 3d-Metal Phosphides. *Adv. Energy Mater.* **2018,** *8* (15), 1703290.
38. Chen, P.; Xu, K.; Tong, Y.; Li, X.; Tao, S.; Fang, Z.; Chu, W.; Wu, X.; Wu, C., Cobalt Nitrides as a Class of Metallic Electrocatalysts for the Oxygen Evolution Reaction. *Inorg. Chem. Front.* **2016,** *3* (2), 236-242.
39. Dutta, A.; Samantara, A. K.; Dutta, S. K.; Jena, B. K.; Pradhan, N., Surface-Oxidized Dicobalt Phosphide Nanoneedles as a Nonprecious, Durable, and Efficient OER Catalyst. *ACS Energy Lett.* **2016,** *1* (1), 169-174.
40. Jin, Z.; Li, P.; Xiao, D., Metallic Co2P Ultrathin Nanowires Distinguished from CoP as Robust Electrocatalysts for Overall Water-Splitting. *Green Chem.* **2015,** *18*.
41. Niu, Y.; Xiao, M.; Zhu, J.; Zeng, T.; Li, J.; Zhang, W.; Su, D.; Yu, A.; Chen, Z., A "Trimurti" Heterostructured Hybrid with an Intimate CoO/CoxP Interface as a Robust Bifunctional Air Electrode for Rechargeable Zn–air Batteries. *J. Mater. Chem. A* **2020**.
42. Deng, Y.-P.; Jiang, Y.; Liang, R.; Zhang, S.-J.; Luo, D.; Hu, Y.; Wang, X.; Li, J.-T.; Yu, A.; Chen, Z., Dynamic Electrocatalyst with Current-driven Oxyhydroxide Shell for Rechargeable Zinc-air Battery. *Nat. Commun.* **2020,** *11* (1), 1952.
43. Lim, D.; Kong, H.; Kim, N.; Lim, C.; Ahn, W.-s.; Baeck, S. H., Oxygen-Deficient $NiFe_2O_4$ Spinel Nanoparticles as an Enhanced Electrocatalyst for the Oxygen Evolution Reaction. *ChemNanoMat* **2019,** *5*.
44. Chauhan, M.; Deka, S., Hollow Cobalt Sulfide Nanoparticles: A Robust and Low-Cost pH-Universal Oxygen Evolution Electrocatalyst. *ACS Appl. Energy Mater.* **2020,** *3* (1), 977-986.

45. Huang, J.; Xu, P.; Gao, T.; Huangfu, J.; Wang, X.-j.; Liu, S.; Zhang, Y.; Song, B., Controlled Synthesis of Hollow Bimetallic Prussian Blue Analog for Conversion into Efficient Oxygen Evolution Electrocatalyst. *ACS Sustainable Chem. Eng.* **2020,** *8* (2), 1319-1328.
46. Nai, J.; Lu, Y.; Yu, L.; Wang, X.; Lou, X. W., Formation of Ni–Fe Mixed Diselenide Nanocages as a Superior Oxygen Evolution Electrocatalyst. *Adv. Mater.* **2017,** *29* (41), 1703870.
47. Han, X.; Zhang, W.; Ma, X.; Zhong, C.; Zhao, N.; Hu, W.; Deng, Y., Identifying the Activation of Bimetallic Sites in NiCo2S4@g-C3N4-CNT Hybrid Electrocatalysts for Synergistic Oxygen Reduction and Evolution. *Adv. Mater.* **2019,** *31* (18), 1808281.
48. Xue, S.; Chen, L.; Liu, Z.; Cheng, H.-M.; Ren, W., NiPS3 Nanosheet–Graphene Composites as Highly Efficient Electrocatalysts for Oxygen Evolution Reaction. *ACS Nano* **2018,** *12* (6), 5297-5305.
49. Liu, J.; Chen, T.; Juan, P.; Peng, W.; Li, Y.; Zhang, F.; Fan, X., Hierarchical Cobalt Borate/MXenes Hybrid with Extraordinary Electrocatalytic Performance in Oxygen Evolution Reaction. *ChemSusChem* **2018,** *11* (21), 3758-3765.